Technical note: Refining $\delta^{15}N$ isotopic fingerprints of local NOx for accurate source identification of nitrate in $PM_{2.5}$

Hao Xiao [1,2], Qinkai Li [3], Shiyuan Ding [2], Wenjing Dai [2], Gaoyang Cui [4], Xiaodong Li [2*]

[1] School of Agriculture and Biology, Shanghai Jiao Tong University, Shanghai, 200240, China;

[2] Institute of Surface-Earth System Science, School of Earth System Science, Tianjin University, Tianjin, 300072, China;

[3] Jiangxi Key Laboratory of Environmental Pollution Control, Jiangxi Academy of Eco-Environmental Sciences and Planning, Nanchang, 330039, China;

[4] The College of Geography and Environmental Science, Henan University, Kaifeng, 475004, China;

***** Correspondence: Xiaodong Li (xiaodong.li@tju.edu.cn)

Contents of this file

Text S1

This study sampled 3 categories of NO_x sources in Tianjin by the active sampling method (Figure S2a) [*Fibiger et al.*, 2014]: coal-fired power plants, gas-fired power plants, biomass combustion, motor vehicle exhaust, iron and steel smelting, and soil release sources (Figure S1). According to data from the Second National Pollution Source Census Bulletin, the three most significant industries in Tianjin in terms of NOx emissions were the electric power and heat production and supply industry (15,700 tonnes), ferrous metal smelting and rolling (14,300 tonnes), and the non-metallic mineral products industry (5,200 tonnes). Collectively, these three industries account for 85% of the NOx emissions from production sector emissions. For example, coal-fired and gas-fired power plants were selected for the electricity and heat production and supply industry, while iron and steel smelting sources were selected for the ferrous metal smelting and rolling processing industry. However, in addition to the above production sectors, actual atmospheric sources of NOx include biomass burning, vehicle exhaust, and soil releases [*Feng et al.*, 2020]. Therefore, the above six NOx sources selected in this study were highly representative.

A vehicle exhaust test station in Tianjin was chosen for bench testing (Figure S2b). NOx emissions from petrol vehicles (n = 19) were collected at the tailpipe outlets, meeting the standard with measured NOx concentrations ranging from 0.1 to 3.6 ppm. Considering the significant range of NOx emission concentrations, a flow rate of 1 L min^{-1} and a sampling duration of 20 min were established in this study to ensure sufficient NO_3^- for concentration determination and $\delta^{15}N$ analysis. Additionally, NOx was collected from two specific atmospheric environments: an urban intersection (n = 18) (Figure S2b) and a tunnel (n = 28) (Figure S2b). The intersection was situated at the junction of Tianjin, with the instrument placed approximately 20 m from the center of the crossroads and at a height of 1.5 m above the ground (Figure S1). Sampling instruments were positioned 30 m from the tunnel entrance (n = 10) and at a midpoint 550 m from the exit (n = 18), with the extraction ports at a height of approximately 1.5 m above ground level. The intersection was determined to be relatively open and illuminated, with NOx concentrations ranging from 0.04 to 0.2 ppm during sampling periods. The sampling flow rate was set to 1.5 L min^{-1}, requiring approximately 120 min to obtain sufficient nitrogen for isotope measurements. The tunnel space is more confined, with weaker lighting, especially at the midpoint. Wind speed mainly depends on the traveling speed of oncoming vehicles. Monitoring data indicated NOx concentrations at the entrance and midpoint of the tunnel ranged from 0.006 to 0.08 ppm and 0.03 to 0.1 ppm, respectively. Consequently, the air extraction flow rate was set to 2 to 3 L min^{-1} for approximately 60 minutes.

In this study, a power plant in Tianjin with an annual coal consumption of approximately 2.5 million tons was selected as a source of NOx from coal combustion (Figure S2c). The power plant employs low-NOx combustion technology, with a combustion temperature of approximately 1400 °C. Flue gas is treated by selective catalytic reduction (SCR) and then discharged, with NOx concentrations at the vent varying between 3.7 and 15.7 ppm, at a temperature of approximately 50 °C. For NOx emission from natural gas combustion, a gas-fired power plant in Tianjin with an annual gas volume of approximately 1.9 billion cubic meters was selected to collect samples in this study. According to monitoring data, the average temperature of the boiler combustion chamber is approximately 1300 °C, with the temperature of the combustion center reaching up to 2200 °C. Exhaust gas is treated by selective catalytic reduction (SCR) technology, with measured NOx concentrations at the emission outlet falling within the range of 8.5 to 9.8 ppm, and the

temperature at the emission outlet being between 90 to 100 °C. The NOx collection at the emission outlet of coal combustion (n = 13) and natural gas combustion (n = 5) in power plants refers to the U.S. EPA Stationary Source Smoke Collection Method (Method 7C). This method involves inserting a 1.5 m long sampling lance into the flue gas outlet during sampling, with a vacuum pump subsequently used to extract the flue gas. To prevent condensation of hot gas inside the absorber tube and the filter cartridge, the heating cartridge was set to 120 °C throughout the sampling process. To obtain sufficient NOx for determining its $\delta^{15}N$, the sampling flow rate was set to 1 L min^{-1} for approximately 20 minutes.

In this study, an iron and steel plant in Tianjin with an annual steel production of approximately 6 million tons was selected to represent iron and steel smelting NOx sources in the region (Figure S2d). Given the diverse processes involved in NOx emissions from the iron and steel industry, including sintering, pelletizing, and hot blast furnace, it is necessary to consider the specific processes of NOx emission at the plant in question. Previous studies have shown that the proportion of pollutants in the flue gas relative to total plant-wide emissions varies considerably across different processes, with the NOx share ranging from 48% to 86% [*Hu et al.*, 2018]. Among these, the sintering and pelletizing processes have relatively low temperatures (1200 to 1400 °C) and emit mainly fuel NOx. In contrast, as an important component of blast furnace smelting, the combustion temperature in the center zone of the hot blast furnace can exceed 1500 °C, with the majority of emissions being thermal type NOx. Therefore, this study focused on collecting flue gas NOx emitted from the sinter tail (n = 7), pellet (n = 5), and hot blast furnace (n = 5) of this steel plant (Figure 2-5). Based on real-time monitoring of NOx concentrations at the vents, NOx concentrations at the sinter tail, pellet, and hot blast furnace vents varied in the ranges of 21.2 to 30.3 ppm, 7.2 to 12.5 ppm, and 4.1 to 6.1 ppm, respectively. The methodology employed in this study was similar to that used in collecting NOx from coal-fired and gas-fired power plant sources. A sampling lance with a length of 1.5 m was extended into the flue gas discharge port, and a vacuum pump was utilized to draw the internal flue gas. To meet the nitrogen content required for determining nitrogen isotopes, a gas flow rate of 1 L min^{-1} was set for the steel smelting NOx source, and a single sample was collected continuously for approximately 20 minutes.

A total of six types of NOx samples from biomass burning emissions were collected for the study (Figure S2e). These included corn stover (n = 3), dried corn cobs (n = 2), old furniture wood (n = 2), elm splits (n = 2), shrub branches (n = 2), and compacted and molded biomass pellets (n = 3). These biomasses were burned in an open-type biomass combustion stove in an actual farming household in Jizhou District, Tianjin, China. Prior to burning each fuel, all previous embers were removed from the combustion furnace [*Shen*, 2012]. Based on real-time monitoring of NOx data emitted from combustion, the compacted-molded biomass combustion emitted the highest concentration of NOx, close to 90 ppm, followed by wood and shrub branches at about 40 ppm, and dried corn cobs and straw at the lowest, about 15 ppm. Therefore, the gas collection flow rate for NOx was set at 0.2 L min^{-1} for approximately 20 minutes.

Soil release sources were differentiated according to two land use types: arable and non-arable land. Given that Tianjin is situated within the North China Plain, wheat cultivation is predominant in the region. Consequently, wheat-cultivated land was the focus of this study. In contrast, non-cultivated land primarily consists of urban green belts and coastal wetlands. NOx samples were collected using the static flux box method (Figure S2f). A one-sided open rectangle

box (590 x 410 x 170 mm) was used to hold approximately 0.24 m^2 of soil underneath the flux box [*Miller et al.*, 2018]. Furthermore, a diaphragm pump was employed to collect NOx released from the soil by establishing a closed-circuit loop at the inlet and outlet, situated at the rectangular diagonal of the flux box. A total of 12 samples of NOx released from soil were collected from agricultural wheat cropland (n = 6), urban greenbelt (n = 3), and coastal wetland soils (n = 3). The arable soil samples were collected from two wheat plots, designated as Plot #1 and Plot #2. Plot #1 was irrigated one week prior to sampling, while Plot #2 was irrigated approximately one month prior. The aforementioned samples were divided into three time periods: morning, midday, and evening. According to a previous study [*Li and Wang*, 2008], the NOx concentration released from soil is typically low compared to other sources. Therefore, the flow rate and duration of NOx collection were set at 1.5 L min^{-1} and 150 min, respectively.

Text S2

The formation pathways of emitted NO_x ($NO+NO_2$) to NO_3^- in polluted cities are complex, which included aqueous-phase and gas-phase reactions. Hence, we assuming that the overall isotope effects (i.e., the ε values in this study) of atmospheric NO_2 conversion to NO_3^-(p) were determined by the contributions of the above two reactions (f_{OH} and f_{N2O5}, respectively) to the oxidations of NO_2 to HNO_3 formation [*Zong et al.*, 2017].

$$\varepsilon = f_{OH} \times \varepsilon_{OH} + f_{N2O5} \times \varepsilon_{N2O5} \quad \text{(Eq 1)}$$

where $f_{OH} + f_{N2O5} = 1$, ε_{OH} and ε_{N2O5} values are isotope fractionations during the above two formation pathways of NO_3^-, respectively.

Since both reactions of NO_2 with OH· and N_2O_5 with H_2O are exchange reactions, both ε_{OH} and ε_{N2O5} values reflect isotope equilibrium effects in respective reaction. Therefore, the ε_{OH} and ε_{N2O5} values can be calculated using the following equation, respectively. (Walters & Michalski 2016).

$$\varepsilon_{OH} = 1000 \times ((15_{\alpha NO2/NO} - 1)(1 - f_{NO2})/((1 - f_{NO2} + (15_{\alpha NO2/NO} \times f_{NO2})) \quad \text{(Eq 2)}$$

$$\varepsilon_{N2O5} = 1000 \times (15_{\alpha N2O5/NO2} - 1) \quad \text{(Eq 3)}$$

where the $^{15}\alpha_{NO2/NO}$ and $^{15}\alpha_{N2O5/NO2}$ value were the equilibrium isotope fractionation factor between NO_2 with NO and N_2O_5 with NO_2, respectively, which is dependent on the temperature (T, as shown in Fig. S3) (Eq 4), and the f_{NO2} is the fraction of NO_2 in the total NO_x.

$$1000\left(15_{\alpha X/Y} - 1\right) = \frac{A}{T^4} \times 10^{10} + \frac{B}{T^3} \times 10^8 + \frac{C}{T^2} \times 10^6 + \frac{B}{T} \times 10^4 \quad \text{(Eq 4)}$$

where A = 3.8834, B = -7.7299, C = 6.0101 and D = -0.17928 for $^{15}\alpha_{NO2/NO}$; and A = 0.69398, B = -1.9859, C = 2.3876 and D = -0.16308 for $^{15}\alpha_{N2O5/NO2}$ [*Walters and Michalski*, 2015].

Additionally, the f_{OH} and f_{N2O5} values were estimated by the ^{18}O fractionations of the above two reactions, respectively [*Zong et al.*, 2017], which can be expressed in Eq 5.

$$\delta^{18}O - NO_3^- = [\delta^{18}O - NO_3^-]_{OH} \times f_{OH} + [\delta^{18}O - NO_3^-]_{N2O5} \times f_{N2O5} \quad \text{(Eq 5)}$$

where $f_{OH} + f_{N2O5} = 1$. The $[\delta^{18}O\text{-}NO_3^-]_{OH}$ and $[\delta^{18}O\text{-}NO_3^-]_{N2O5}$ were calculated by the following equations, respectively.

$$[\delta^{18}O - NO_3^-]_{OH} = \frac{2}{3} \times [\delta^{18}O - NO_2]_{OH} + \frac{1}{3} \times [\delta^{18}O - OH]_{OH} \quad \text{(Eq 6)}$$

$$[\delta^{18}O - NO_3^-]_{N2O5} = \frac{5}{6} \times [\delta^{18}O - N_2O_5] + \frac{1}{6} \times [\delta^{18}O - H_2O] \quad \text{(Eq 7)}$$

where the $[\delta^{18}O\text{-}NO_2]_{OH}$ and $[\delta^{18}O\text{-}OH]_{OH}$ values were calculated by the Eq 8 and Eq 9, respectively. The $\delta^{18}O\text{-}H_2O$ values were estimated as the $\delta^{18}O$ values of tropospheric water vapor (-12.5±17.6‰), and the $\delta^{18}O\text{-}N_2O_5$ values were 126.4±7.1‰ [*Walters and Michalski*, 2016].

$$[\delta^{18}O - NO_2]_{OH} = 1000 \times \left(18_{\alpha NO2/NO} - 1\right) \times \frac{1 - f_{NO2}}{(1 - f_{NO2}) + \left(18_{\alpha NO2/NO} \times f_{NO2}\right)} + [\delta^{18}O - NO_x] \quad \text{(Eq 8)}$$

$$[\delta^{18}O - OH]_{OH} = (\delta^{18}O - H_2O) + 1000 \times (18_{\alpha OH/H2O} - 1) \quad \text{(Eq 9)}$$

In Eq 8 and Eq 9, the $^{18}\alpha_{NO/NO2}$ and $^{18}\alpha_{OH/H2O}$ (expressed as the $^{18}\alpha_{X/Y}$) values were calculated by the following equation (Eq 10).

$$1000\left(18_{\alpha X/Y} - 1\right) = \frac{A}{T^4} \times 10^{10} + \frac{B}{T^3} \times 10^8 + \frac{C}{T^2} \times 10^6 + \frac{B}{T} \times 10^4 \quad \text{(Eq 10)}$$

where A = -0.04129, B = 1.1605, C = -1.8829 and D = 0.74723 for $^{18}\alpha_{NO/NO2}$; and A = 2.1137, B = -3.8026, C = 2.2653 and D = 0.5941 for $^{18}\alpha_{H2O/OH}$ [*Walters and Michalski*, 2015].

Text S3

The study employed the uncertainty index (UI_{90}), as defined previously by other researchers, in order to characterise the uncertainty inherent in results concerning the contributions of NOx sources [*Ji et al.*, 2022; *Zhang et al.*, 2024]. This index is designed to express the strength of uncertainty under conditions of a high probability, specifically at 90%. The datasets in question exhibit a normal distribution, with the vast majority of data points falling within the ranges of 90% to 95% and 95% to 100%. The majority of proportional contributions occur within the cumulative frequency range of 5% to 95%. Consequently, there is a more rapid and pronounced increase in cumulative frequency. Therefore, extreme values in the small probability range (10%) can be mitigated through the utilisation of UI90. The formula for UI90 is presented below:

$$UI_{90} = (P_{95\%} - P_{5\%})/(0.95 - 0.05) \quad \text{(Eq 11)}$$

where the P95% and P5% were the proportional contributions at the 95% and 5% cumulative probabilities, respectively. Low uncertainty, as indicated by small UI90 values, suggests a stable source contribution result [*Zhang et al.*, 2024].

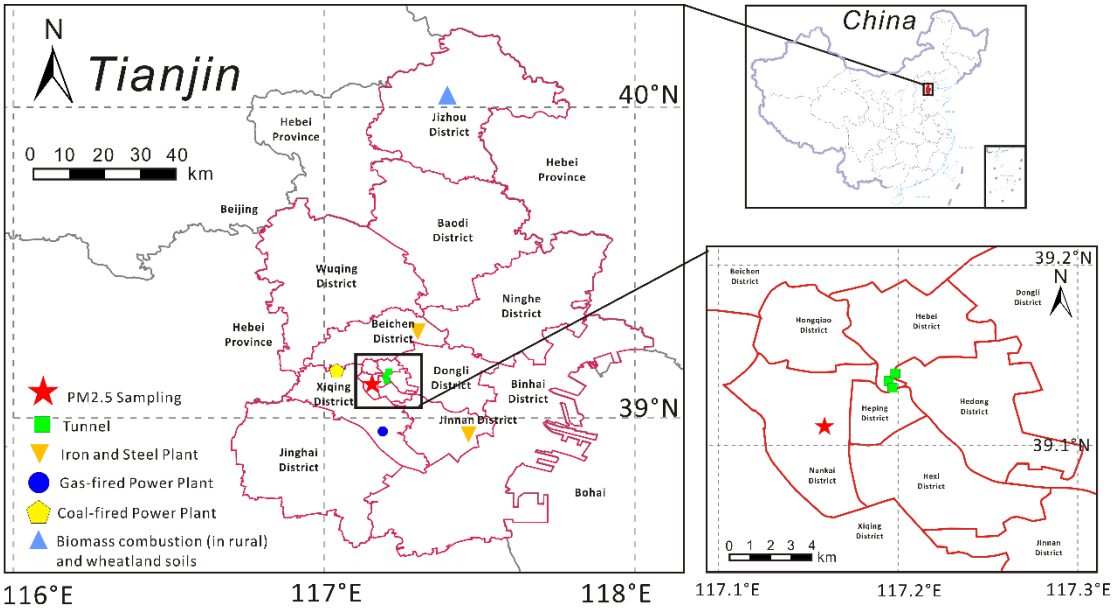

Figure S1 Map of $PM_{2.5}$ and NOx source sampling locations

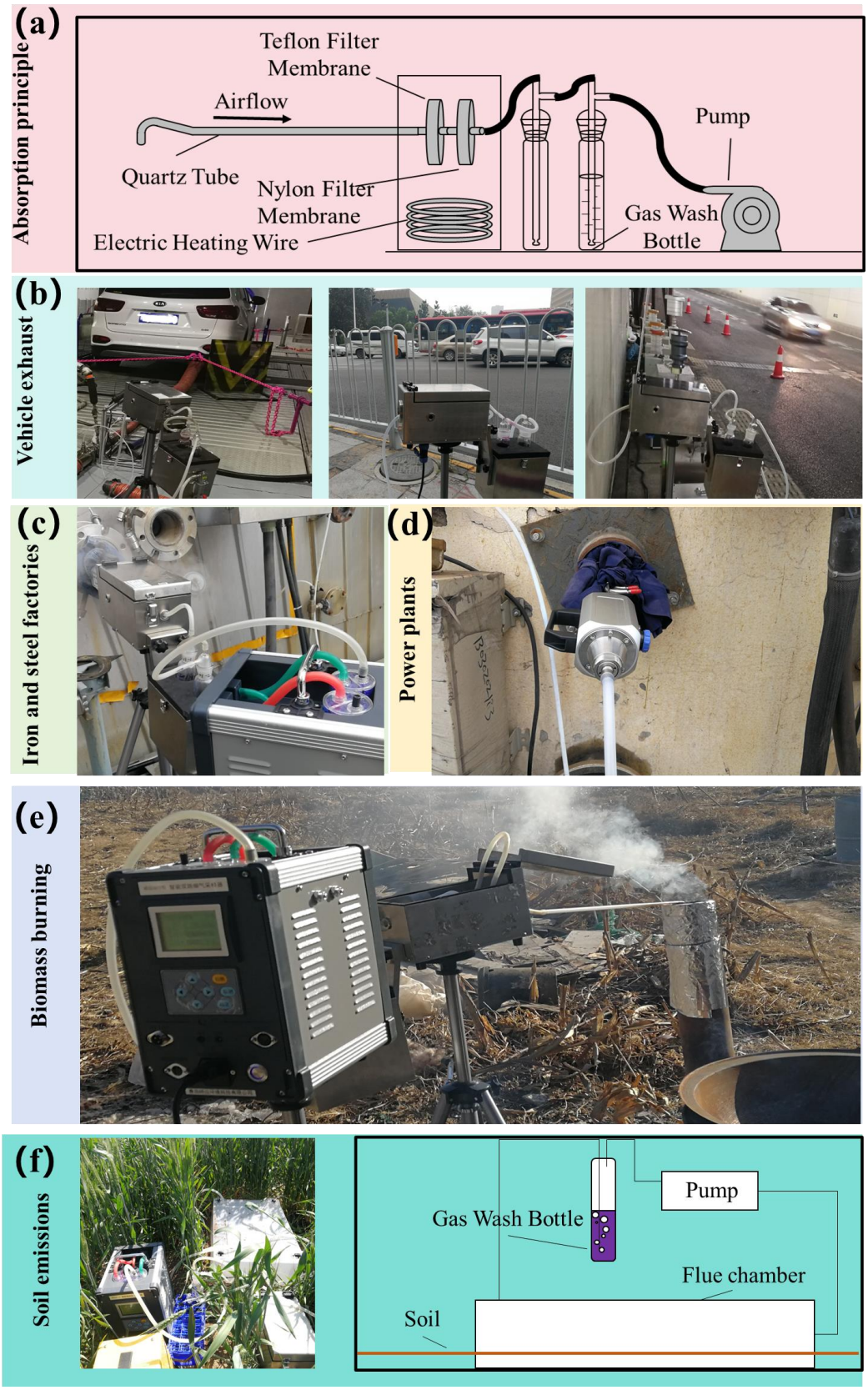

Figure S2 NO_x sampling device diagram of this study

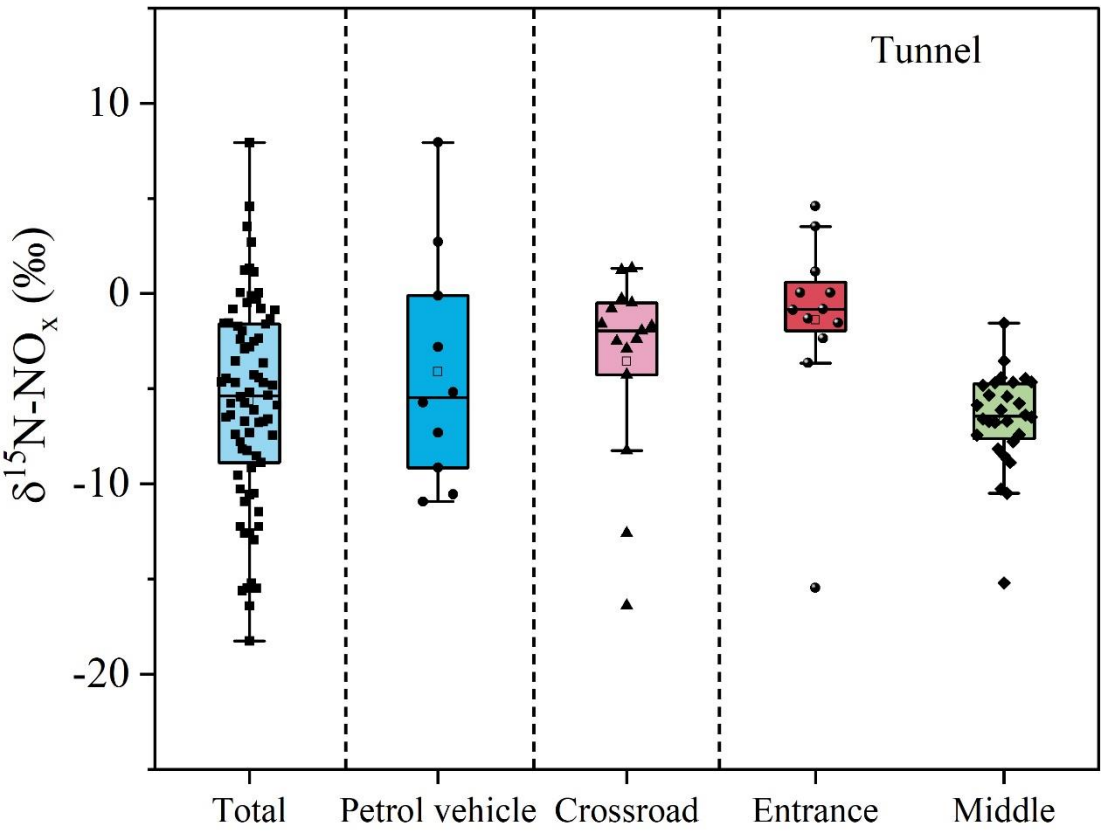

Figure S3 The $\delta^{15}N$ values of NO_x from vehicle exhaust emission at different sampling sites

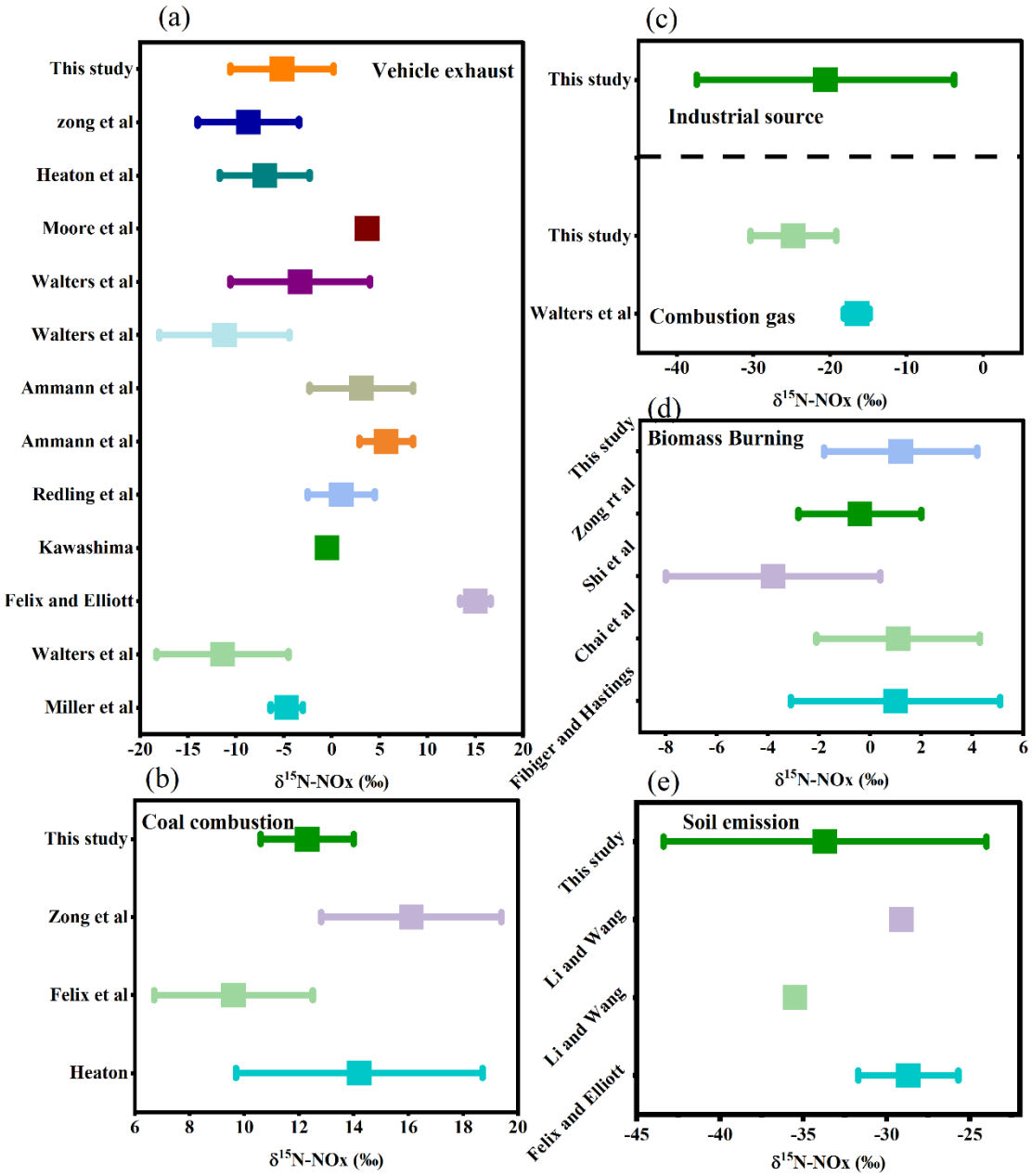

Fig S4 Comparison of $\delta^{15}N$ values in NO_x sources between this study and previous studies [*Felix and Elliott*, 2013; 2014; *Felix et al.*, 2015; *Felix et al.*, 2012; *Fibiger and Hastings*, 2016; *Hastings et al.*, 2009; *Li and Wang*, 2008; *Walters et al.*, 2015a; *Walters et al.*, 2015b]

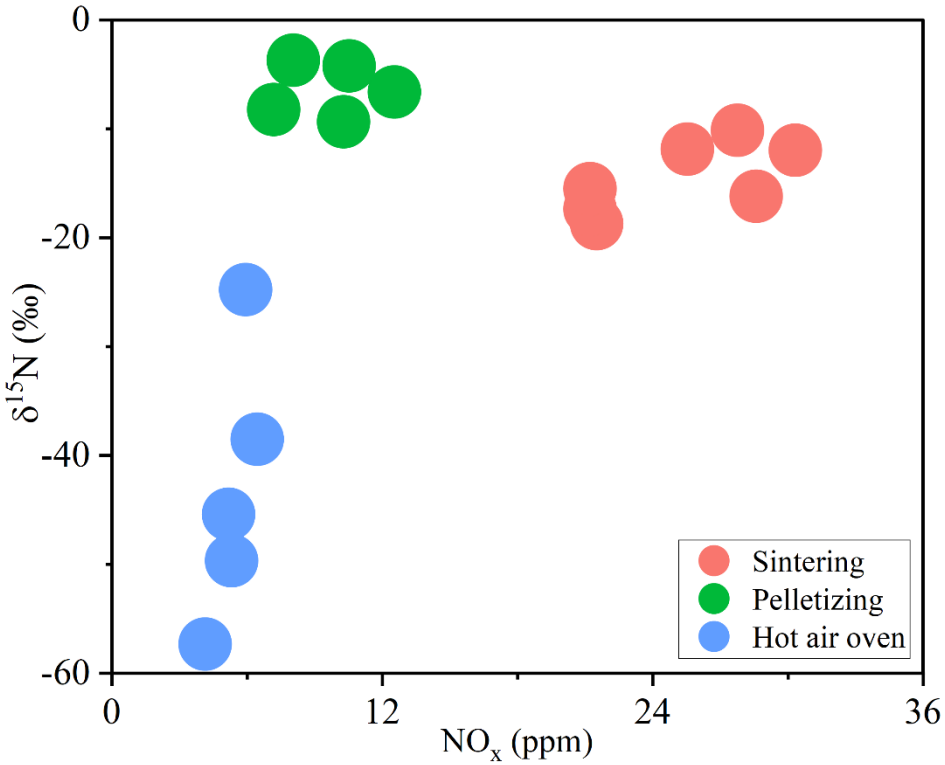

Figure S5 The concentrations and $\delta^{15}N$ values of NOx emissions from different processes in steel smelting

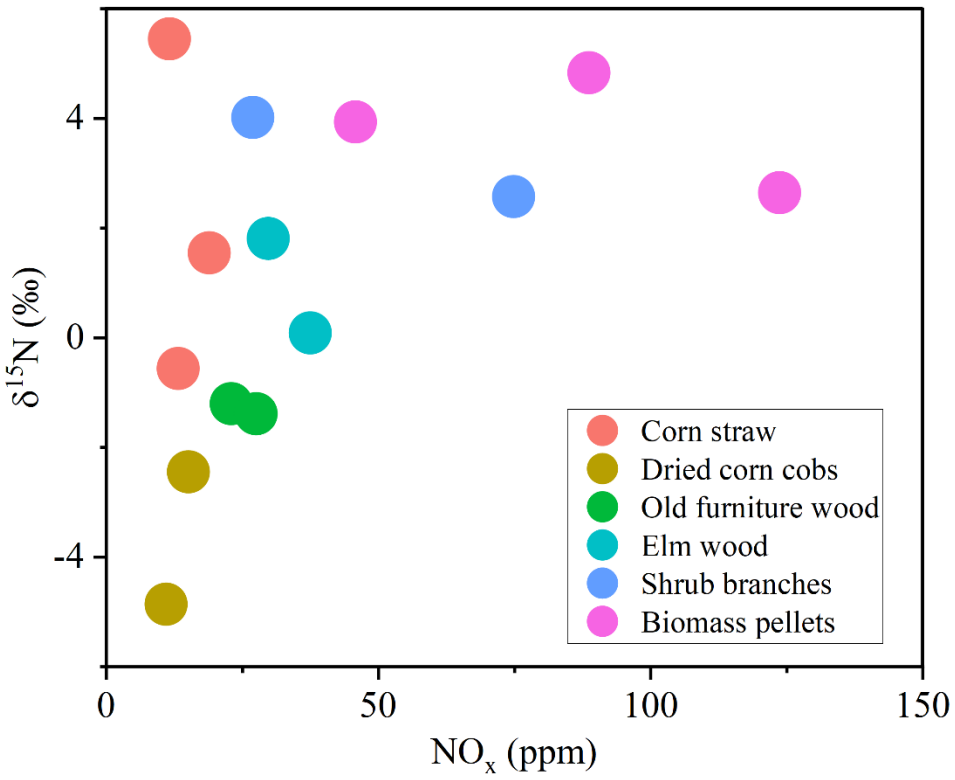

Figure S6 The concentrations and $\delta^{15}N$ values of NOx emissions from different biomass burning

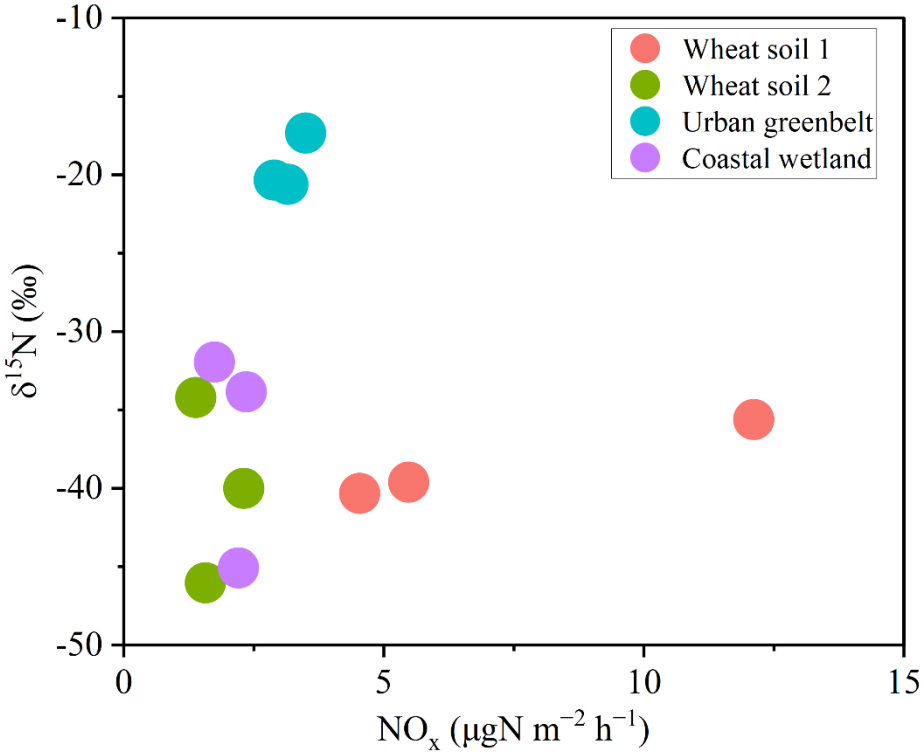

Figure S7 The concentrations and $\delta^{15}N$ values of NOx emissions from different soil types

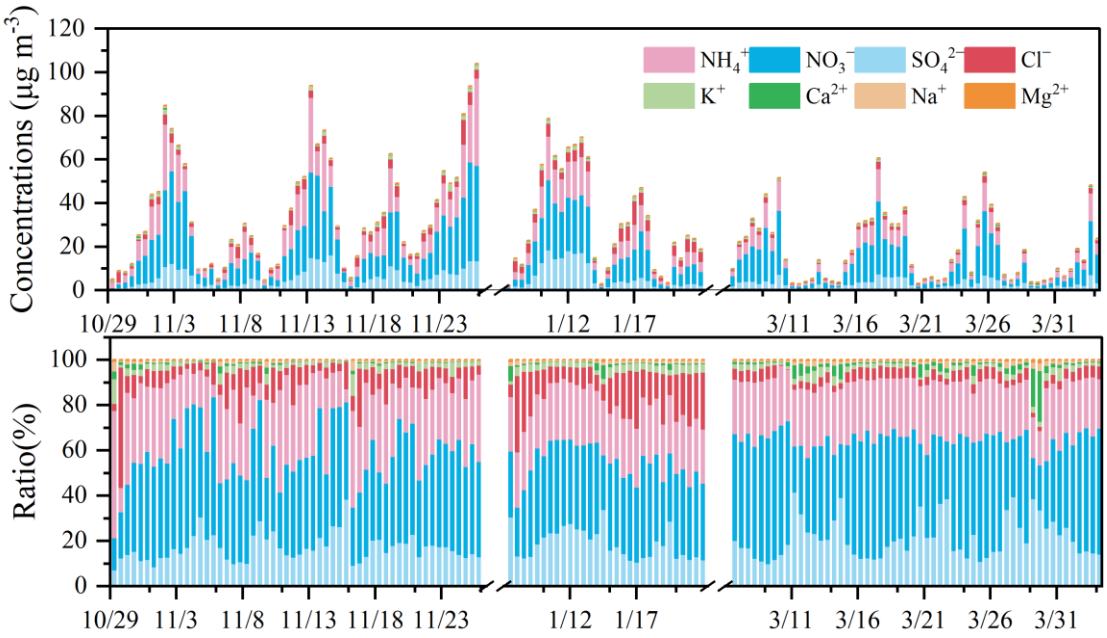

Figure S8 Time series of the concentrations and percentage in major inorganic ions in $PM_{2.5}$ during sampling periods

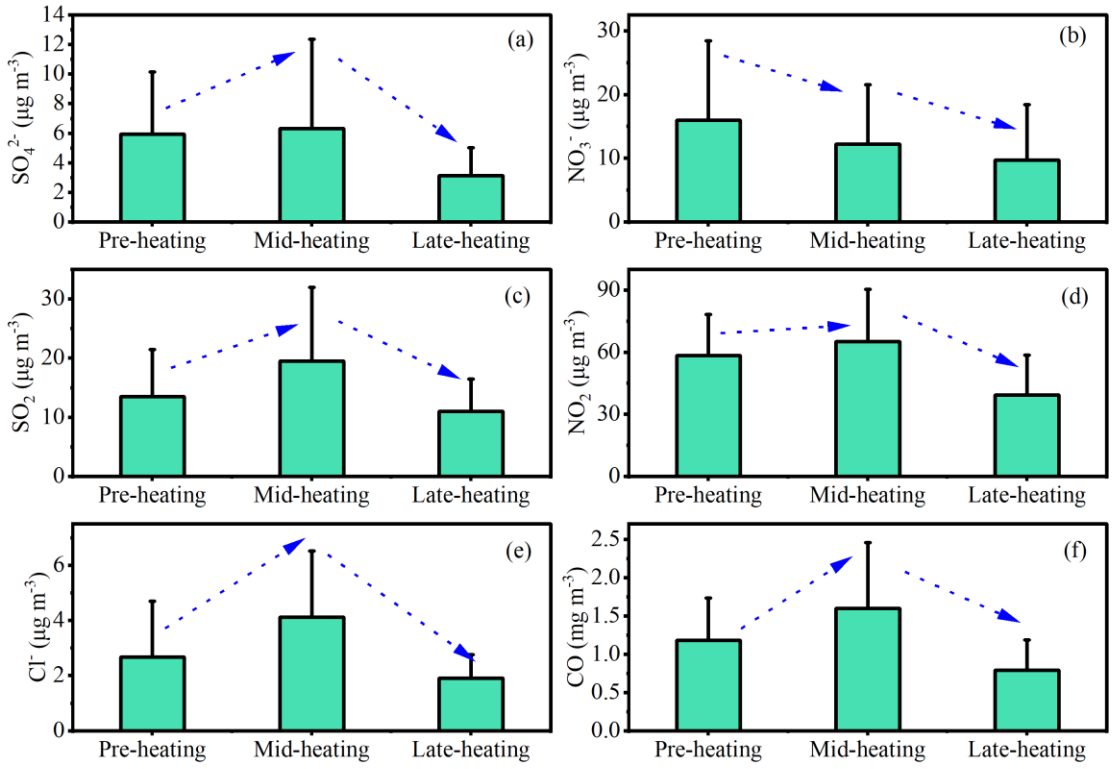

Fig S9 Changes in the concentrations of trace factors related to coal combustion over different sampling periods

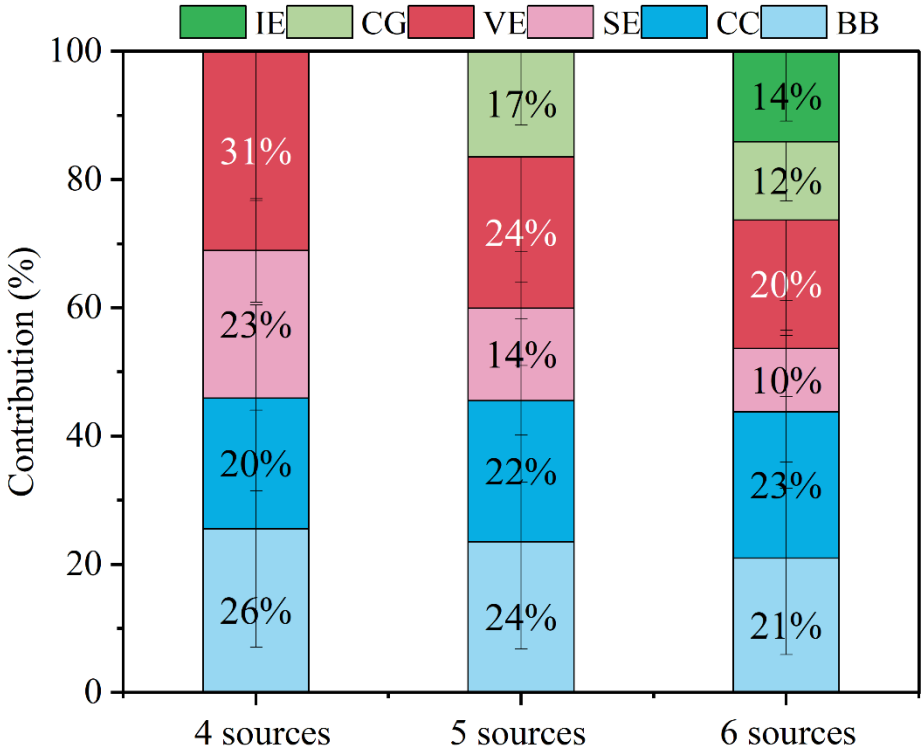

Figure S10 The contribution fraction of NO_3^- sources in $PM_{2.5}$ in Tianjin was estimated using the $\delta^{15}N$ values obtained from this study for four, five, and six NOx sources. The IE represents the industrial emission, the CG represents the natural gas combustion, the VE represents the vehicles exhaust, the SE represents the soil emission, the CC represents the coal combustion, the BB represents the biomass burning.

Table S1 The pollutant concentrations and meteorological parameters in Tianjin urban areas at different sampling stages for 2018 ~ 2019 (av ± std)

	All days	2018.11	2019.01	2019.03
RH (%)	35.2 ± 17.5	46.2 ± 14.8	31.1 ± 20.3	26.3 ± 11.6
T (℃)	8.7 ± 5.2	9.7 ± 3.0	1.0 ± 2.9	11.8 ± 3.7
WS (m s^{-1})	1.7 ± 0.9	1.3 ± 0.6	1.6 ± 0.8	2.1 ± 1.0
NO_2 (μg m^{-3})	52.3 ± 23.4	58.4 ± 19.9	65.1 ± 25.2	39.3 ± 19.2
SO_2 (μg m^{-3})	13.8 ± 8.9	13.5 ± 7.9	19.5 ± 12.5	11.0 ± 5.5
CO (mg m^{-3})	1.1 ± 0.7	1.2 ± 0.6	1.6 ± 0.9	0.8 ± 0.4
O_3 (μg m^{-3})	42.2 ± 28.2	30.3 ± 22.4	22.4 ± 18.0	62.7 ± 23.6

Table S2 The probability density functions (PDFs) in relative contribution of each source to NO_3^- in $PM_{2.5}$ at QOMS tested by four, five and six emission sources.

	Biomass burning											
4 sources	-0.5	-0.5										
5 sources	-0.6	-0.5	Coal combustion									
6 sources	/	-0.5										
4 sources	-0.5	-0.8	-0.5	-0.4								
5 sources	-0.3	-0.4	-0.4	-0.4	Vehicles exhaust							
6 sources	/	-0.3	/	-0.4								
4 sources	0.01	0.01	0.7	0.7	-0.8	-0.8						
5 sources	0.01	0.03	0.5	0.3	-0.4	-0.3	Soil emission					
6 sources	/	0.01	/	0.4	/	-0.1						
4 sources		/	/	/		/	/	/				
5 sources	0.02	-0.1	0.01	0.3	-0.3	-0.3	-0.6	-0.6	Natural gas combustion			
6 sources		0.01		0.01		-0.2		-0.4				
4 sources	/	/	/	/	/	/	/	/	/	/		
5 sources	/	/	/	/	/	/	/	/	/	/	Industrial emission	
6 sources	/	0.1	/	0.1	/	-0.2	/	-0.3	/	-0.2		
	Previous study	This study	Previous study	This study	Previous study	This study	Previous study	This study	Previous study	This study	Previous study	This study

Note: The "/" represents no data

Reference

Felix, J. D., and Elliott, E. M. (2013), The agricultural history of human-nitrogen interactions as recorded in ice core $\delta^{15}N\text{-}NO_3^-$, *Geophys. Res. Lett.*, *40*, 1642-1646, doi:https://doi.org/10.1002/grl.50209.

Felix, J. D., and Elliott, E. M. (2014), Isotopic composition of passively collected nitrogen dioxide emissions: Vehicle, soil and livestock source signatures, *Atmos. Environ.*, *92*, 359-366, doi:https://doi.org/10.1016/j.atmosenv.2014.04.005.

Felix, J. D., Elliott, E. M., Avery, G. B., Kieber, R. J., Mead, R. N., Willey, J. D., and Mullaugh, K. M. (2015), Isotopic composition of nitrate in sequential Hurricane Irene precipitation samples: Implications for changing NOx sources, *Atmos. Environ.*, *106*, 191-195, doi:https://doi.org/10.1016/j.atmosenv.2015.01.075.

Felix, J. D., Elliott, E. M., and Shaw, S. L. (2012), Nitrogen isotopic composition of coal-fired power plant NO_x: influence of emission controls and implications for global emission inventories, *Environ. Sci. Technol.*, *46*(6), 3528-3535, doi:https://doi.org/10.1021/es203355v.

Feng, X., Li, Q., Tao, Y., Ding, S., Chen, Y., and Li, X. (2020), Impact of coal replacing Project on atmospheric fine aerosol nitrate loading and formation pathways in urban Tianjin: Insights from chemical composition and ^{15}N and ^{18}O isotope ratios, *Sci. Tot. Environ.*, *708*(15), 134797, doi:https://doi.org/10.1016/j.scitotenv.2019.134797.

Fibiger, D. L., and Hastings, M. G. (2016), First measurements of the nitrogen isotopic composition of NOx from biomass burning, *Environ. Sci. Technol.* , *50*(21), 11569-11574, doi:https://doi.org/10.1021/acs.est.6b03510.

Fibiger, D. L., Hastings, M. G., Lew, A. F., and Peltier, R. E. (2014), Collection of NO and NO_2 for Isotopic Analysis of NO_x Emissions, *Anal. Chem.*, *86*(24), 12115-12121, doi:https://doi.org/10.1021/ac502968e.

Hastings, M. G., Jarvis, J. C., and Steig, E. J. (2009), Anthropogenic impacts on nitrogen isotopes of ice-core nitrate, *Science*, *324*(5932), 1288-1288, doi:https://doi.org/10.1126/science.1170510.

Hu, B., YE, H., Wang, Z., Zhou, Z. a., and Xiang, X. (2018), NOx emission behavior and control method of grate-kiln pelletizing process (in chinese), *China Metallurgy*, *28*(04), 66-70, doi:https://doi.org/10.13228/j.boyuan.issn1006-9356.20170261.

Ji, X., Shu, L., Chen, W., Chen, Z., Shang, X., Yang, Y., Dahlgren, R. A., and Zhang, M. (2022), Nitrate pollution source apportionment, uncertainty and sensitivity analysis across a rural-urban river network based on $\delta^{15}N/\delta^{18}O\text{-}NO_3^-$ isotopes and SIAR modeling, *J. Hazard. Mater.*, *438*, 129480, doi:https://doi.org/10.1016/j.jhazmat.2022.129480.

Li, D., and Wang, X. (2008), Nitrogen isotopic signature of soil-released nitric oxide (NO) after fertilizer application, *Atmos. Environ.*, *42*(19), 4747-4754, doi:https://doi.org/10.1016/j.atmosenv.2008.01.042.

Miller, D. J., Chai, J., Guo, F., Dell, C. J., Karsten, H., and Hastings, M. G. (2018), Isotopic composition of in situ soil NOx emissions in manure-fertilized cropland, *Geophys. Res. Lett.*, *45*(21), 12,058-012,066, doi:https://doi.org/10.1029/2018GL079619.

Shen, G. (2012), Emission factors of carbonaceous particulate matter and polycyclic aromatic hydrocarbons from residential solid fuel combustions (in chinese), Doctor thesis, Peking University.

Walters, W. W., Goodwin, S. R., and Michalski, G. (2015a), Nitrogen stable isotope composition ($\delta^{15}N$)

of vehicle-emitted NO_x, *Environ. Sci. Technol.*, *49*(4), 2278-2285, doi:https://doi.org/10.1021/es505580v.

Walters, W. W., and Michalski, G. (2015), Theoretical calculation of nitrogen isotope equilibrium exchange fractionation factors for various NO_y molecules, *Geochim. Cosmochim. Acta.*, *164*(7), 284-297, doi:https://doi.org/10.1016/j.gca.2015.05.029.

Walters, W. W., and Michalski, G. (2016), Theoretical calculation of oxygen equilibrium isotope fractionation factors involving various NO_y molecules, radical OH, and H_2O and its implications for isotope variations in atmospheric nitrate, *Geochim. Cosmochim. Acta.*, *191*, 89-101, doi:https://doi.org/10.1016/j.gca.2016.06.039.

Walters, W. W., Tharp, B. D., Fang, H., Kozak, B. J., and Michalski, G. (2015b), Nitrogen isotope composition of thermally produced NOx from various fossil-fuel combustion sources, *Environ. Sci. Technol.*, *49*(19), 11363-11371, doi:https://doi.org/10.1021/acs.est.5b02769.

Zhang, W., Wu, F., Luo, X., Song, L., Wang, X., Zhang, Y., Wu, J., Xiao, Z., Cao, F., Bi, X., and Feng, Y. (2024), Quantification of NOx sources contribution to ambient nitrate aerosol, uncertainty analysis and sensitivity analysis in a megacity, *Sci. Tot. Environ.*, *926*, 171583, doi:https://doi.org/10.1016/j.scitotenv.2024.171583.

Zong, Z., Wang, X., Tian, C., Chen, Y., Fang, Y., Zhang, F., Li, C., Sun, J., Li, J., and Zhang, G. (2017), First assessment of NO_x sources at a regional background site in North China using isotopic analysis linked with modeling, *Environ. Sci. Technol.*, *51*(11), 5923-5931, doi:https://doi.org/10.1021/acs.est.6b06316.